remote sensing

MDPI

Article

Differences in Vegetation Productivity Loss and Recovery Dynamics Between Flash and Conventional Droughts in Central Asia

Jiaqi Guo [1,2], Yaning Chen [1,2,*], Yupeng Li [2], Yuhui Yang [1], Gonghuan Fang [2], Zhi Li [2], Fan Sun [2] and Jiaorong Qian [1]

[1] Xinjiang Laboratory of Lake Environment and Resources in Arid Zone, College of Geographic Science and Tourism, Xinjiang Normal University, Urumqi 830054, China
[2] Xinjiang Institute of Ecology and Geography, Chinese Academy of Sciences, Urumqi 830011, China
* Correspondence: chenyn@ms.xjb.ac.cn

Highlights

What are the main findings?

- Flash droughts occurred approximately twice as frequently and exhibited a 3.5-fold higher mean intensity than conventional droughts, inducing greater regional mean GPP decline across Central Asia.
- Post-drought vegetation recovery times were significantly prolonged following flash droughts in croplands, grasslands, and forests, whereas shrublands exhibited comparable recovery durations under both regimes.

What are the implications of the main findings?

- Cumulative soil moisture replenishment during the recovery period serves as the primary governing factor (contributing > 60%) for accelerating vegetation recovery across drylands.
- These findings provide empirical benchmarks and scientific references for post-drought ecological vulnerability assessment and climate-adaptive ecosystem management in Central Asia.

Abstract

Flash droughts (FDs) develop rapidly through abrupt soil moisture depletion, yet their impacts on dryland vegetation productivity and recovery remain poorly understood. Here, we compared FDs and conventional droughts (CDs) across Central Asia using ERA5-Land soil moisture from 1980 to 2022 and GLASS gross primary productivity (GPP) from 2000 to 2022. Integrating spatiotemporal analyses with XGBoost and SHAP, we quantified GPP losses and recovery durations across four vegetation types and identified their primary drivers. Both drought types increased significantly in frequency, with FDs occurring nearly twice as often and exhibiting a 3.5-fold higher mean intensity than CDs. Consequently, FDs caused a greater overall GPP decline magnitude of 1.875 versus 1.602 standardized anomaly units and prolonged recovery to 50.79 days compared with 42.19 days under CDs. At the biome level, post-FD recovery was significantly longer in croplands, grasslands, and forests, while shrublands showed comparable recovery times between regimes. The XGBoost models reliably simulated recovery time, identifying cumulative recovery-period soil moisture anomaly as the dominant driver contributing over 60% under both regimes, alongside drought intensity and recovery-period atmospheric conditions. These findings

Academic Editor: Akira Iwasaki

Received: 26 October 2026
Revised: 19 November 2026
Accepted: 23 November 2026
Published: 25 November 2026

Copyright: © 2026 by the authors. Licensee MDPI, Basel, Switzerland. This article is an open access article distributed under the terms and conditions of the Creative Commons Attribution (CC BY) license.

highlight the severe ecological threat of rapid soil desiccation and provide scientific references for dryland restoration and climate adaptation.

Keywords: Central Asia; flash drought; conventional drought; gross primary productivity; recovery time

1. Introduction

Under the ongoing acceleration of global climate change, the occurrence frequency, duration, and damage severity of extreme drought events have increased considerably, causing profound disturbances to the carbon sink capacity and structural integrity of terrestrial ecosystems [1–3]. Arid and semi-arid regions cover over 40% of the global land surface. These regions are widely characterized by scarce water resources, fragile vegetation cover, and high climatic sensitivity, making them prone to ecological degradation and desertification under severe moisture deficits [4,5]. Located in the hinterland of the Eurasian continent, Central Asia is a quintessential temperate inland dryland. In recent decades, its warming rate has reached nearly twice the global average, accompanied by enhanced evapotranspiration and persistent desiccation of surface soils [6,7]. Although Central Asian vegetation plays a fundamental role in regulating regional hydrothermal equilibrium and sustaining ecological security barriers [8], escalating hydrothermal imbalances have triggered frequent grassland degradation and cropland yield losses, posing severe challenges to the realization of the United Nations Sustainable Development Goal (SDG) 15.3 regarding land degradation neutrality [9].

In recent years, global drought patterns have undergone profound shifts. Flash drought (FD) events, which feature rapid onset and high development intensity, have increased markedly and become a focal research topic in climatology and ecology [10,11]. Unlike conventional drought (CD), which relies on prolonged precipitation deficits and evolves slowly over months or years, flash drought is typically driven by the co-occurrence of severe rainfall deficits and surging atmospheric evaporative demand. This combination can deplete soil moisture in an abrupt manner within a few weeks [12,13]. Recent global assessments demonstrate that more than 74% of global terrestrial lands have experienced a transition from slow-developing droughts toward flash droughts since 1951 [11]. While past investigations focused on humid hotspots with high baseline soil water content, recent evidence demonstrates that flash droughts are spreading into semi-arid and arid non-hotspot regions, where lower baseline soil water content exacerbates rapid soil desiccation [14]. In Central Asia, researchers have recognized the elevated incidence of sub-seasonal droughts; however, most existing studies still rely on monthly or annual meteorological indicators [11,15] or focus solely on flash droughts [16], failing to differentiate the fundamental distinctions between flash and conventional droughts at sub-seasonal scales. Consequently, an in-depth understanding of the long-term spatiotemporal evolution of both drought regimes across Central Asia is still lacking.

The abrupt onset of flash drought exerts a severe physiological shock on terrestrial ecosystems, frequently exceeding plant physiological tolerance thresholds and triggering precipitous drops in productivity [17–19]. During a flash drought event, surging atmospheric water demand drives rapid plant transpiration that depletes root-zone moisture before stomatal regulation can mount an effective defense. This leads to xylem hydraulic failure, photosynthetic disruption, and leaf wilting, ultimately resulting in significant declines in gross primary productivity (GPP) [3,20,21]. Nevertheless, drought disturbance to ecosystems is not limited to the acute damage phase; the post-drought ecological recovery trajectory is equally vital for sustaining long-term ecosystem stability

and resilience [18,22,23]. Vegetation recovery time reflects the persistence of drought legacy effects and the vulnerability of ecosystems when confronting secondary disturbances [24,25]. If the vegetation recovery time exceeds the recurrence interval between successive droughts, unhealed physiological injuries will compound, leaving vegetation in a persistent sub-healthy state or potentially triggering irreversible ecological degradation [5,26]. Furthermore, due to considerable disparities in rooting depth, hydraulic architecture, and life-history strategies, post-drought recovery trajectories vary substantially across different biomes [18,27,28]. In Central Asia, existing investigations have primarily examined monthly GPP response lag times to flash droughts [8], evaluated ecosystem water-use efficiency responses solely under flash droughts without comparison to conventional droughts [16], or assessed annual-scale productivity recovery following prolonged meteorological droughts without resolving sub-seasonal drought regimes [29]. Consequently, an integrated sub-seasonal assessment that simultaneously compares acute GPP decline magnitude, post-drought recovery duration, and their biome-specific divergences between flash and conventional droughts across Central Asia remains absent.

The vegetation recovery process is co-regulated by the attributes of the preceding drought event and hydrothermal conditions during the recovery period [22,25,30]. Previous studies have demonstrated that soil moisture replenishment during the recovery period is an essential prerequisite for restoring plant water balance and physiological function [23]. Concurrently, atmospheric factors such as air temperature, precipitation, solar radiation, vapor pressure deficit (VPD), and actual evapotranspiration (ET) also exert vital modulatory effects on the recovery of photosynthetic capacity [31,32]. Nevertheless, under the respective impacts of flash and conventional droughts, the explicit mechanisms connecting vegetation recovery time with various environmental and drought attributes remain unclear. Coupling the Extreme Gradient Boosting (XGBoost) algorithm with the SHapley Additive exPlanations (SHAP) framework can resolve multicollinearity among variables and accurately quantify the relative contributions of individual drivers to vegetation recovery duration [32,33].

Therefore, this study focuses on Central Asia as an ecologically sensitive and fragile dryland. Based on ERA5-Land soil moisture data from 1980 to 2022 and GLASS GPP products from 2000 to 2022, we conducted an assessment of vegetation productivity impairment and subsequent recovery under flash versus conventional droughts at a 0.1° spatial resolution and an 8-day temporal scale. Specifically, this study aims to address three critical scientific questions: (1) How do flash droughts and conventional droughts differ in the spatiotemporal patterns of their occurrence frequency, duration, and intensity across Central Asia over the past 43 years? (2) How do forests, croplands, shrublands, and grasslands contrast in their responses to flash droughts and conventional droughts in terms of the magnitude of GPP decline and post-drought recovery duration? (3) What are the relative importance and functional roles of drought properties and recovery-period hydrothermal factors in shaping vegetation recovery time, and how do these roles diverge between the two drought regimes? This study aims to clarify the divergent impacts of flash and conventional droughts on Central Asian ecosystems, providing a scientific foundation for constructing ecological security barriers and implementing climate-adaptive management across arid and semi-arid regions.

2. Materials and Methods

2.1. Study Area

Central Asia encompasses five nations: Kazakhstan, Uzbekistan, Turkmenistan, Tajikistan, and Kyrgyzstan, as shown in Figure 1. Situated in the inland heart of Eurasia and spanning 46°E to 87°E in longitude and 35°N to 55°N in latitude, the region covers a total land area of approximately 4 million km². The topography is complex and diverse, bounded by prominent mountain systems in the east and southeast, and dominated by expansive low-lying plains and desert basins in the west, displaying an overall elevation gradient that decreases gradually from east to west [34]. Central Asia is characterized by a typical temperate continental arid and semi-arid climate, featuring pronounced spatial variations in hydroclimatic regimes. Annual precipitation ranges from less than 100 mm in desert lowlands to over 1000 mm in high-mountain zones, while mean annual air temperature varies greatly across the territory [15,35]. Governed by climatic and topographic gradients, land cover exhibits marked spatial heterogeneity. Grasslands and sparse vegetation dominate the landscape, whereas croplands, shrublands, and temperate forests occur locally, concentrated primarily across the northern rainfed agricultural belt and river valley oases [36].

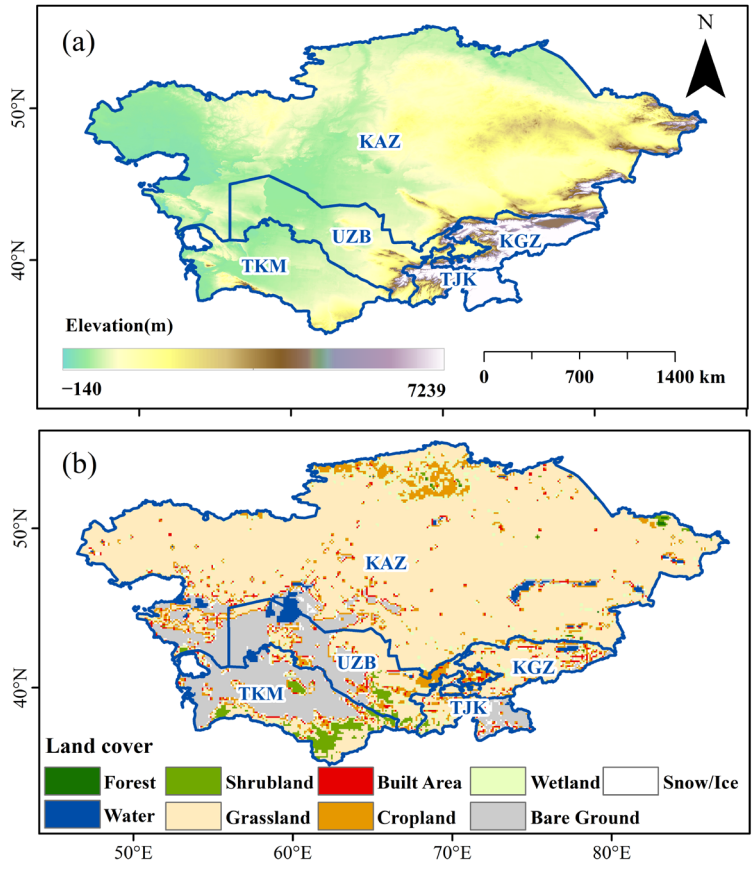

Figure 1. Study area of Central Asia. (**a**) Spatial distribution of elevation; (**b**) land cover types.

2.2. Data Sources

2.2.1. Soil Moisture Data

Soil moisture data were obtained from the consolidated-release ERA5-Land reanalysis dataset produced by the European Centre for Medium-Range Weather Forecasts (ECMWF). It has a native spatial resolution of 0.1° and covers the period from 1950 to the present with an hourly temporal resolution [37]. Built-in assimilation-based

quality control for this dataset was completed by ECMWF. ERA5-Land provides volumetric soil water content across three vertical depth intervals: 0 to 7 cm, 7 to 28 cm, and 28 to 100 cm. To reflect the effective water volume accessible to plant root systems, a depth-weighted average integration was applied to generate root-zone soil moisture from 0 to 100 cm, denoted as $SM_{0–100cm}$:

$$SM_{0-100}cm = 0.07 \times SM_1 + 0.21 \times SM_2 + 0.72 \times SM_3, \quad (1)$$

where SM_1, SM_2, and SM_3 represent the volumetric soil water content of the 0–7 cm, 7–28 cm, and 28–100 cm soil layers, respectively; the coefficients 0.07, 0.21, and 0.72 denote the thickness weight proportions of these three vertical layers within the 0–100 cm root-zone profile.

2.2.2. Vegetation Gross Primary Productivity Data

Vegetation productivity dynamics were characterized using Version 6.0 of the Global Land Surface Satellite gross primary productivity product (GLASS12E01 V6.0) spanning 2000–2022 [38]. Derived from the Eddy Covariance-Light Use Efficiency (EC-LUE) model and validated against global FLUXNET eddy covariance tower observations, this product features an original spatial resolution of 500 m and an 8-day temporal resolution. Pixel quality flags embedded in the product were utilized to mask observations contaminated by heavy clouds, aerosols, or snow/ice cover, and invalid/negative values were removed. Raw digital numbers were multiplied by the official scaling factor of 0.01 to obtain the average daily GPP for each 8-day period (in g C m^{-2} day^{-1}). The data were then spatially aggregated and resampled to the unified 0.1° grid using bilinear interpolation. As GPP is a continuous surface variable, bilinear interpolation is suitable for GPP resampling and can reduce positional biases and block-like artifacts caused by the nearest-neighbor method.

2.2.3. Meteorological Data

Meteorological variables—including 2 m air temperature (T), 2 m dewpoint temperature (T_{dew}), precipitation, surface downward solar radiation, and actual evapotranspiration—were extracted from the ERA5-Land reanalysis dataset, with non-terrestrial pixels and major water bodies masked as NoData across the study domain. To align with the 8-day temporal resolution of the GLASS GPP product, daily data were temporally aggregated into 46 fixed 8-day intervals per calendar year using arithmetic means of daily values. As ERA5-Land provides continuous gap-free records over land surfaces, no additional gap-filling was performed on valid terrestrial pixels during the aggregation process. Saturated vapor pressure (SVP, in kPa), actual vapor pressure (AVP, in kPa), and vapor pressure deficit (VPD, in kPa) [39] were computed as follows:

$$SVP = 0.6108 \times \exp\left(\frac{17.27 \times T}{T + 237.3}\right), \quad (2)$$

$$AVP = 0.6108 \times \exp\left(\frac{17.27 \times T_{dew}}{T_{dew} + 237.3}\right), \quad (3)$$

and

$$VPD = SVP - AVP, \quad (4)$$

where T and T_{dew} represent the 2 m air temperature (°C) and dewpoint temperature (°C), respectively.

2.2.4. Land Cover Data

Land cover classifications were derived from the 30 m Global Land Cover product with Fine Classification System (GLC_FCS30D) spanning 1985–2022 [40]. This dataset provides 5-year interval maps prior to 2000 and annual dynamic maps from 2000 to 2022. To account for temporal land-cover transitions, year-specific dynamic layers were matched annually to vegetation responses over the 2000–2022 period. Four dominant biomes were extracted: forests, croplands, shrublands, and grasslands. The 30 m data were aggregated to the 0.1° grid using majority-class resampling to align with ERA5-Land and GPP.

To eliminate spatial mismatch and high-frequency temporal noise while capturing sub-seasonal drought dynamics and vegetation responses, all datasets were standardized to a 0.1° by 0.1° spatial grid and an 8-day temporal step. All analytical computations were restricted to the active vegetation growing season from April to October.

2.3. Methods

To evaluate the divergent ecological impacts of flash and conventional droughts across Central Asia, an integrated methodological framework was established (Figure 2). The full 43-year ERA5-Land record (1980–2022) was utilized to construct empirical percentiles and examine long-term drought climatology. In contrast, all vegetation response evaluations and XGBoost–SHAP attribution analyses were strictly restricted to the 2000–2022 overlapping period, with drought events occurring during 1980–1999 excluded to ensure temporal consistency across datasets.

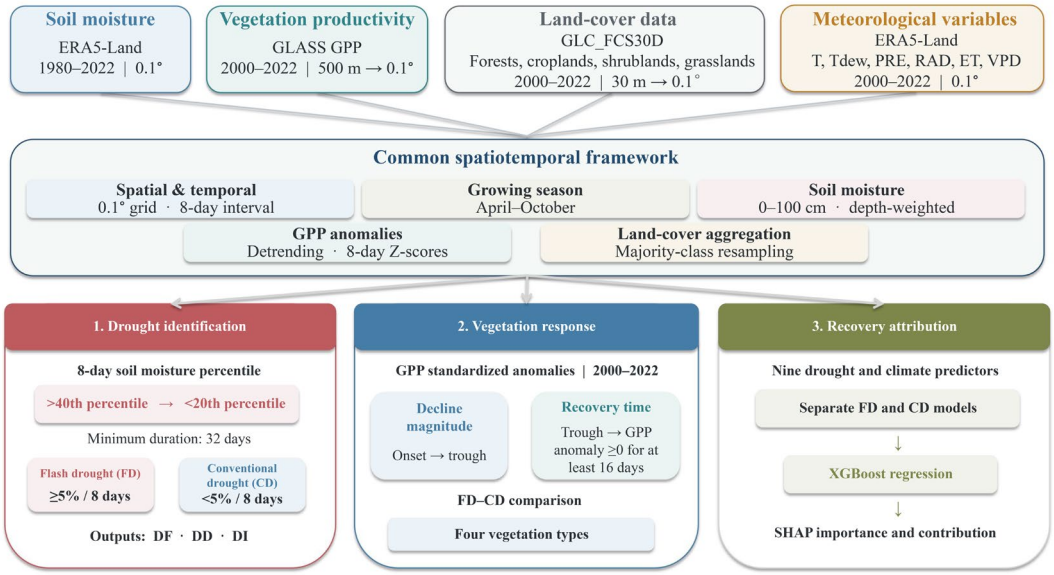

Figure 2. Workflow of this study.

2.3.1. Identification of Flash and Conventional Droughts

To remove the interference of seasonal cycles and avoid sampling bias from individual anomalous years, an empirical cumulative distribution function (CDF) was constructed for each pixel across each 8-day window over the 1980–2022 baseline period, transforming raw root-zone soil moisture into standardized percentiles ranging from 0% to 100%.

Following the soil-moisture-percentile-based drought identification framework proposed by Yuan et al. [41] and Zhang et al. [42], flash and conventional drought events were detected from 8-day soil moisture percentile time series for the April-to-October growing season. Within this framework, the 40th percentile denotes the normal-to-wet baseline that signals the onset of soil desiccation, and the 20th percentile acts as the

drought threshold for triggering vegetation water stress [12,43]. Furthermore, an onset-rate threshold of 5 percentile points per 8-day interval paired with a 32-day minimum event duration, a scheme previously implemented across Northern Hemisphere ecosystems ranging from humid to arid and semi-arid zones, was adopted to screen out short-lived moisture fluctuations that exert little ecological influence [42].

Specifically, qualifying drought events were delineated and classified according to two rules, as illustrated in Figure 3:

(1) Drought Definition and Lifespan Threshold: A drought event began when the soil moisture percentile dropped from at or above 40% to below 20% and terminated once it recovered to or above 20%; transient fluctuations remaining below 20% were treated as intra-event variability. If soil moisture fell below 20% again without first recovering to at least 40% to re-establish a pre-drought baseline, the subsequent dry spell was not merged with the preceding event and was excluded from both drought inventories, as were right-censored episodes extending past October. Each complete drought event was required to persist for at least 32 days.

(2) Classification by Onset Depletion Rate: Each qualifying event was classified according to the average rate of soil moisture decline during its onset phase, defined from the last step at or above 40% to the first crossing below 20%. Episodes with an average onset decline rate of at least 5% per 8 days were classified as flash droughts, whereas those with rates below 5% per 8 days were classified as conventional droughts. To evaluate classification robustness, sensitivity tests were also performed using alternative onset thresholds of 4.0% and 6.0% per 8 days.

To characterize the spatial and temporal behavior of both drought regimes, three fundamental drought metrics were calculated for each pixel:

(1) Drought frequency (DF, events·yr^{-1}): defined as the multi-year average number of drought events occurring per year.

(2) Drought duration (DD, days): defined as the total elapsed time from drought onset to termination.

(3) Drought intensity (DI, %): defined as the multi-year average deficit depth, calculated as the difference between the 20% drought threshold and the soil moisture percentile during the drought duration.

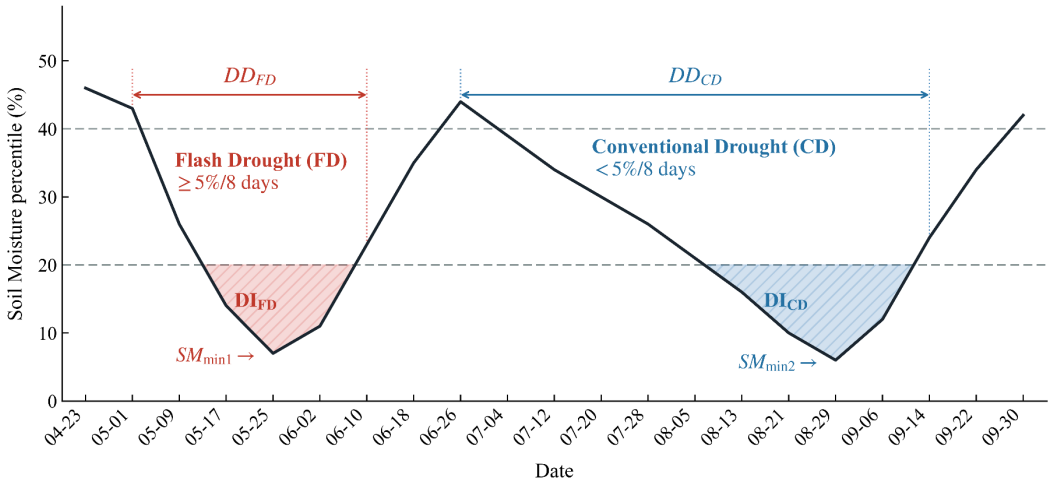

Figure 3. Schematic illustration of identification criteria for flash drought (FD) and conventional drought (CD).

2.3.2. Quantification of Vegetation Decline Magnitude and Recovery Time

To eliminate the influence of long-term climate warming trends and intra-annual phenological cycles on vegetation productivity, pixel-wise linear detrending was performed on the growing-season GPP series. Climate-standardized anomalies, expressed as Z-scores, were calculated for each 8-day interval:

$$GPP_{anomaly,t} = \frac{GPP_{detrended,t} - \mu_s}{\sigma_s}, \quad (5)$$

where μ_s and σ_s represent the multi-year mean and standard deviation of detrended GPP for the corresponding 8-day calendar interval, respectively.

To exclude random biological fluctuations unrelated to drought stress, we retained only valid events with valid GPP records, normal growth at drought onset ($GPP_{anomaly} \geq 0$), and sustained damage thereafter. Sustained damage was defined as negative GPP anomalies persisting for at least two consecutive 8-day steps. Of the 135,377 flash droughts (FDs) and 75,408 conventional droughts (CDs) identified for 2000–2022, 94,031 FDs and 51,743 CDs were excluded under these screening criteria, leaving 41,346 FDs and 23,665 CDs for subsequent analysis.

(1) Decline magnitude, reported in standardized anomaly units, quantifies the peak acute damage to vegetation productivity. It is defined as the difference between the standardized GPP anomaly at drought onset and the minimum trough anomaly within the drought response window. All 41,346 retained FD and 23,665 CD events were included in the calculation of decline magnitude, regardless of subsequent recovery status.

(2) Recovery time, reported in days, represents the time required for vegetation functional recovery. It is defined as the number of days elapsed from the timing of the maximum GPP damage trough until the standardized GPP anomaly first returns to and remains ≥0 for at least 16 consecutive days. This criterion indicates recovery to the detrended multi-year climatological mean rather than a return to the instantaneous pre-drought productivity level. When subsequent droughts occur after soil moisture recovers to ≥40%, tracking for such interrupted events continues, so compounding delays are incorporated into the estimated recovery duration. After excluding 10,332 FDs and 6903 CDs that failed to recover before the end of the growing season or reached the 180-day maximum tracking limit without meeting the recovery requirement, 31,014 FDs and 16,762 CDs were retained for recovery-time analysis.

2.3.3. Trend Analysis and Statistical Significance Tests

Ordinary least squares (OLS) linear regressions were applied to quantify decadal trends, and statistical significance was evaluated via two-tailed Student's t-tests using Newey–West heteroscedasticity and autocorrelation consistent (HAC) robust standard errors to account for temporal autocorrelation. The non-parametric Mann–Whitney U test was applied to evaluate differences in GPP decline magnitude and recovery time between flash and conventional droughts at the regional scale and separately within each vegetation biome, namely forests, croplands, shrublands, and grasslands. Pearson correlation and linear regression analyses were used to assess the dependency of vegetation recovery time on productivity decline magnitude.

2.3.4. Attribution of Recovery Time Drivers Using XGBoost and SHAP

To evaluate the relative importance of environmental and drought factors on vegetation recovery time under flash and conventional droughts, machine learning models were established by combining the XGBoost Regressor with the SHAP interpretability algorithm. Taking vegetation recovery time as the target variable, we constructed a feature matrix containing nine predictor variables for 30,768 flash droughts

and 16,687 conventional droughts spanning 2000–2022. This matrix comprised three drought attributes: drought intensity (DI), drought frequency (DF), and drought duration (DD); and cumulative standardized anomalies of six hydrothermal variables during the vegetation recovery period: soil moisture (SMrec), precipitation (PRErec), air temperature (TEMrec), vapor pressure deficit (VPDrec), solar radiation (RADrec), and actual evapotranspiration (ETrec).

Separate XGBoost models were constructed for flash and conventional droughts with 100 trees, a maximum depth of 5, and a learning rate of 0.05, as cross-validated tuning confirmed that higher complexity did not improve generalization. To eliminate spatiotemporal autocorrelation, model performance (R^2) was evaluated using a 5 × 5 Leave-Location-and-Time-Out cross-validation (LLTO-CV) scheme, which partitioned grid cells into five K-Means spatial blocks and 2000–2022 into five contiguous multi-year blocks, excluding both held-out space and time blocks during training. Finally, the validated models were refitted on all samples, and the SHAP TreeExplainer was applied to quantify driver importance in days and relative contribution percentages.

3. Results

3.1. Spatiotemporal Distributions of Flash and Conventional Droughts

To investigate the spatiotemporal patterns and trends of flash and conventional droughts across Central Asia, drought frequency (DF), duration (DD), and intensity (DI) were derived from 1980–2022 ERA5-Land soil moisture percentiles using the onset depletion-rate framework. Prior to examining these regional drought characteristics, a sensitivity analysis was performed to evaluate alternative flash-drought onset-rate thresholds of 4.0% and 6.0% per 8 days relative to the 5.0% baseline (Table 1). Spatial frequency distributions showed strong consistency across tested thresholds, justifying the adoption of the 5.0% baseline for all subsequent analyses.

Table 1. Spatial consistency and sensitivity analysis of drought frequency across Central Asia under alternative flash-drought onset-rate thresholds (4.0%/8 d and 6.0%/8 d) relative to the 5.0%/8 d baseline.

Drought Type	Comparison	Pearson r	*p*-Value (Pearson)	Spearman ϱ	*p*-Value (Spearman)	Spatial Overlap
FD	4.0%/8 d vs. 5.0%/8 d	0.98	<0.001	0.98	<0.001	96.20%
FD	6.0%/8 d vs. 5.0%/8 d	0.98	<0.001	0.97	<0.001	94.88%
FD	4.0%/8 d vs. 6.0%/8 d	0.95	<0.001	0.95	<0.001	91.28%
CD	4.0%/8 d vs. 5.0%/8 d	0.88	<0.001	0.89	<0.001	90.84%
CD	6.0%/8 d vs. 5.0%/8 d	0.93	<0.001	0.93	<0.001	96.06%
CD	4.0%/8 d vs. 6.0%/8 d	0.77	<0.001	0.78	<0.001	87.26%

Based on the validated 5.0% per 8-day baseline, Figure 4 illustrates the pronounced spatiotemporal divergences and interannual trends of DF, DD, and DI across Central Asia over the past 43 years.

Regarding occurrence frequency, the multi-year average frequency of flash droughts was 0.138 events per year, displaying a spatial distribution that was higher in the north and east and lower in the south and west. High-frequency areas were concentrated across the temperate grasslands of northern and eastern Kazakhstan, whereas hyper-arid sectors in the south witnessed few flash droughts, as shown in Figure 4a. In comparison, conventional droughts showed a relatively uniform spatial distribution across the region but had a lower overall mean frequency of 0.072 events per year, as shown in Figure 4d. The occurrence frequency of flash droughts was approximately 1.9 times that of conventional droughts. Over the 1980–2022 period, the occurrence frequencies of flash

droughts and conventional droughts exhibited significant upward trends, with $p < 0.05$ and $p < 0.001$, respectively, as shown in Figure 4g. The frequency of flash droughts increased at a rate of 0.050 events per year per decade, whereas conventional droughts increased at 0.032 events per year per decade.

The duration of conventional droughts was longer than that of flash droughts across the entire study area, as shown in Figure 4b,e. The mean duration of flash droughts was 54.67 days, with 90.68% of the study area experiencing flash drought durations shorter than 85 days. In contrast, the mean duration of conventional droughts reached 88.74 days. Over the past four decades, both categories showed significant lengthening trends, as shown in Figure 4h. Flash drought duration extended at a rate of 2.86 days per decade with $p < 0.01$, while conventional drought duration extended at 3.45 days per decade with $p < 0.05$.

The soil moisture deficit depth caused by flash droughts was deeper than that caused by conventional droughts across most of Central Asia, as shown in Figure 4c,f. The multi-year average intensity of flash droughts reached 4.15%, with higher values in the northern grasslands and eastern foothills. In contrast, the intensity of conventional droughts remained weaker across the region, with an average value of 1.17%. The mean intensity of flash droughts was approximately 3.5 times that of conventional droughts. In terms of temporal trends, the intensities of both drought types exhibited non-significant upward tendencies with $p > 0.05$, as shown in Figure 4i, with increase rates of 0.08% per decade for flash droughts and 0.04% per decade for conventional droughts.

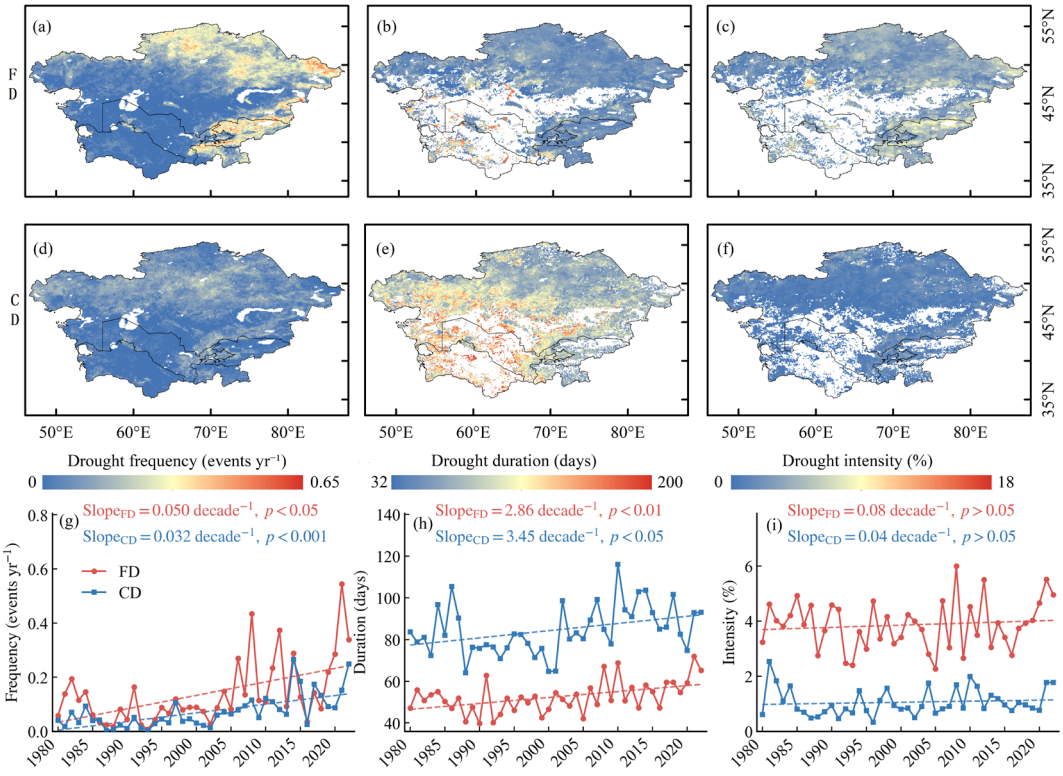

Figure 4. Spatiotemporal patterns and interannual trends of flash droughts (FDs) and conventional droughts (CDs) across Central Asia (1980–2022). Panels (**a**–**f**) show multi-year mean frequency (events · yr^{-1}), duration (days), and drought intensity (%) for FD (**a**–**c**) and CD (**d**–**f**) during the April–October growing season; blank areas denote non-terrestrial/water pixels or zero-event cells. Panels (**g**–**i**) illustrate regional interannual variations and Newey–West HAC OLS trends. Regional frequency (**g**) averages across all terrestrial cells (0 events · yr^{-1} for non-drought cells), whereas duration (**h**) and intensity (**i**) are conditionally averaged across drought-affected cells only.

3.2. Vegetation Decline and Recovery Under Flash and Conventional Droughts

From 2000 to 2022, the magnitude of the decline in vegetation GPP under flash droughts and conventional droughts showed spatial variation, as illustrated in Figure 5. Under both drought regimes, areas with higher GPP decline magnitudes were situated mainly in northern and northeastern Kazakhstan and around the southeastern Tien Shan mountains, whereas areas with lower decline magnitudes were located in parts of the southern and southwestern sectors, as shown in Figure 5a,b. While both drought types exhibited similar spatial configurations of productivity loss, zones with larger decline magnitudes were more concentrated under flash droughts. The overall event-mean decline magnitude caused by flash droughts was 1.875 standardized anomaly units, which was higher than the value of 1.602 recorded for conventional droughts ($p < 0.001$). Regarding temporal variations, the productivity decline magnitude caused by flash droughts increased at a rate of 0.016 standardized anomaly units per decade with $p > 0.05$, whereas conventional droughts exhibited a downward trend of −0.081 per decade with $p > 0.05$, as shown in Figure 5c.

Different vegetation biomes showed distinct damage responses, as shown in Figure 5d. Forests, croplands, and grasslands suffered significantly higher mean GPP decline magnitudes under flash droughts than under conventional droughts ($p < 0.001$). Specifically, the mean decline magnitude, expressed in standardized anomaly units, for forests under flash droughts was 2.328, compared with 1.895 under conventional droughts; grasslands exhibited values of 1.842 versus 1.606; and croplands recorded 1.799 versus 1.632. In contrast, shrublands experienced a significantly higher average decline magnitude under conventional droughts than under flash droughts, with values of 1.588 versus 1.406 ($p < 0.001$), showing a contrasting response pattern relative to the other three vegetation types.

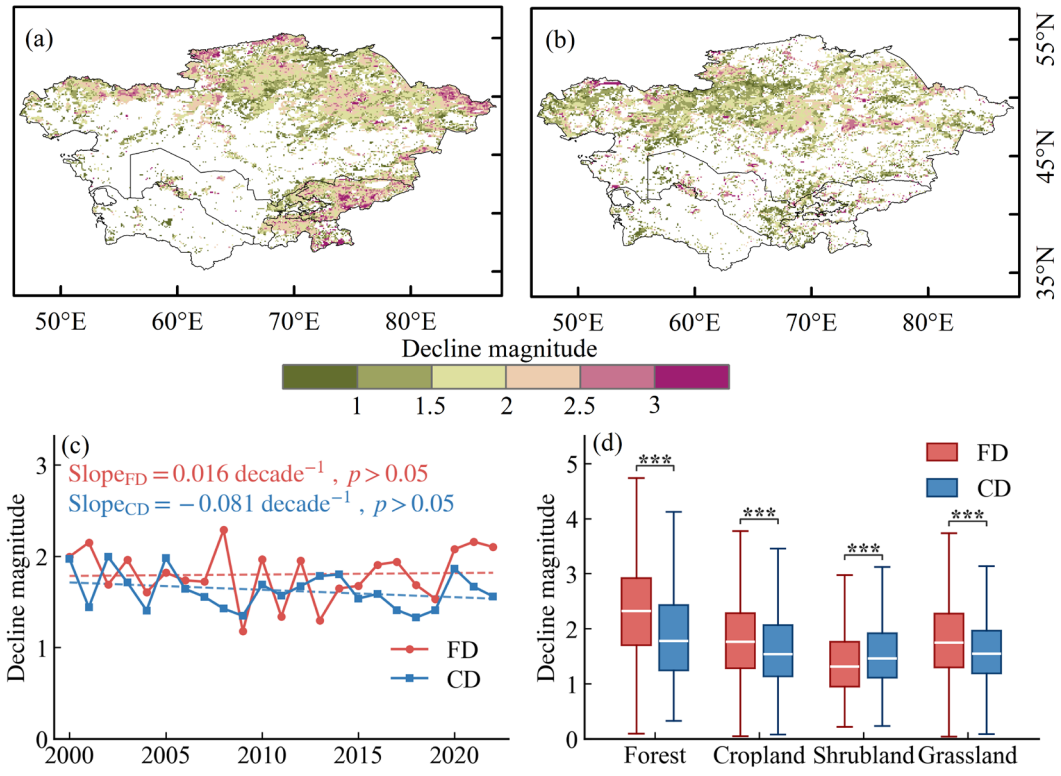

Figure 5. Spatiotemporal patterns in the magnitude of vegetation GPP decline across Central Asia (2000–2022). Panels (**a**,**b**) show multi-year mean decline magnitudes under flash droughts (FD) and conventional droughts (CD); blank areas denote non-vegetated pixels or regions without qualifying events. Panel (**c**) shows regional interannual trends evaluated via Newey–West HAC OLS

regressions. Panel (**d**) compares GPP decline across biomes (boxplots show median, IQR, and 1.5× IQR whiskers). Sample sizes (N, FD/CD): forest (4916/301), cropland (12,828/5498), shrubland (237/722), and grassland (21,563/15,693). Significance levels are determined using the two-sided Mann–Whitney U test: *** $p < 0.001$.

From 2000 to 2022, vegetation GPP recovery time across Central Asia also showed spatial differentiation, as shown in Figure 6a,b. Regions requiring longer recovery times following flash droughts were located in northern and northeastern Kazakhstan and around the southeastern Tien Shan mountains. Under conventional droughts, areas with longer recovery durations were more dispersed. The overall event-mean recovery time following flash droughts was 50.79 days, compared with 42.19 days under conventional droughts ($p < 0.001$). Over the 2000–2022 period, recovery times following both drought types showed upward trends, with rates of 4.566 days per decade and 5.612 days per decade, respectively, both with $p > 0.05$, as shown in Figure 6c.

Different vegetation biomes exhibited variations in recovery time, as illustrated in Figure 6d. Compared with conventional droughts, flash droughts induced significantly longer mean recovery times in croplands, grasslands, and forests ($p < 0.001$), whereas the difference in shrublands was not statistically significant ($p > 0.05$). Croplands and grasslands experienced the longest recovery times: croplands averaged 54.22 days under flash droughts and 41.77 days under conventional droughts, whereas grasslands required 51.55 days and 44.16 days, respectively. Forests required 43.76 days versus 35.13 days. Shrublands exhibited the shortest recovery durations, averaging 25.33 days under flash droughts and 23.76 days under conventional droughts.

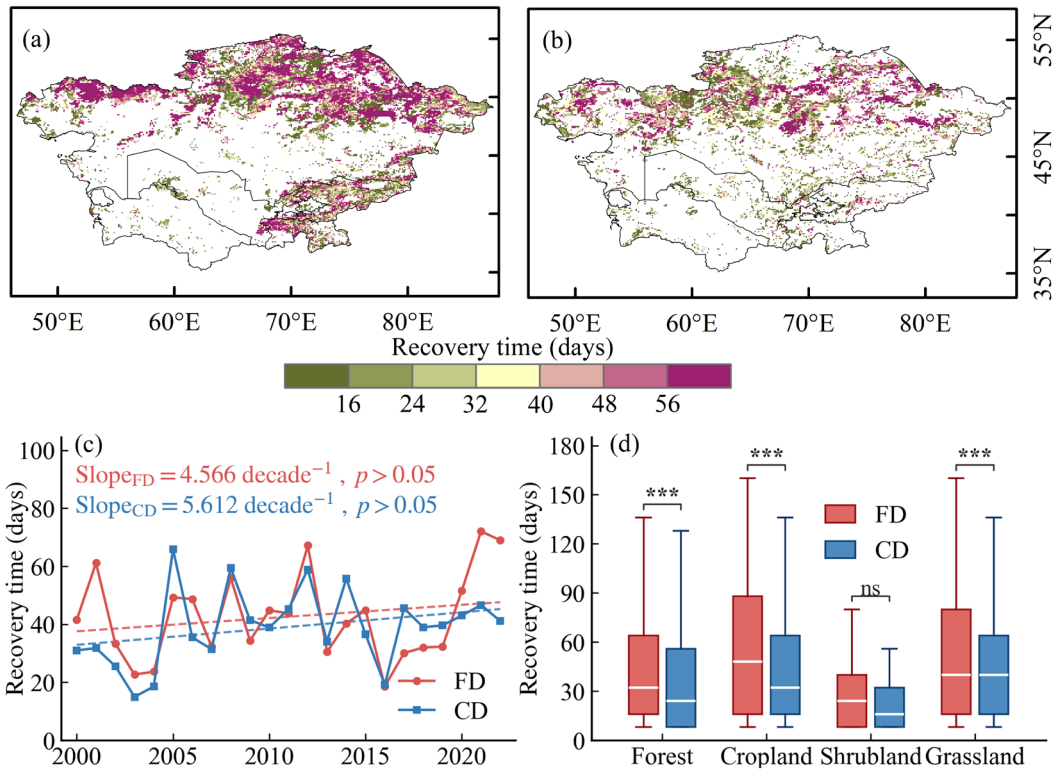

Figure 6. Spatiotemporal patterns of vegetation GPP recovery time across Central Asia (2000–2022). Panels (**a**,**b**) show multi-year mean recovery times under FD and CD; blank areas denote non-vegetated pixels, no qualifying events, or episodes not recovering within the tracking window. Panel (**c**) shows regional interannual trends evaluated via Newey–West HAC OLS regressions. Panel (**d**) compares recovery times across biomes. Sample sizes (N, FD/CD): forest (3546/197),

cropland (10,154/4325), shrubland (138/430), and grassland (16,057/10,987). Significance levels are determined using the two-sided Mann–Whitney U test: *** $p < 0.001$ and ns indicates $p \geq 0.05$.

To examine the relationship between productivity loss severity and recovery duration, linear regression analysis was performed between GPP decline magnitude and recovery time. Under both drought regimes, vegetation recovery time extended significantly as the GPP decline magnitude increased ($p < 0.001$), as illustrated in Figure 7a. The sensitivity slope reached 11.40 under flash droughts, noticeably higher than the 10.34 observed under conventional droughts, indicating that deepening productivity loss had a stronger prolonging effect on recovery duration following flash droughts. Evaluating recovery times across three productivity decline severity tiers, defined as mild for values below 1.5, moderate for values from 1.5 to 2.5, and severe for values above 2.5, confirmed that post-flash drought recovery times were systematically longer than post-conventional drought recovery times. Furthermore, the recovery time discrepancy between flash and conventional droughts widened progressively with increasing decline severity, reaching 1.5, 8.1, and 14.7 days for mild, moderate, and severe declines, respectively (Figure 7b).

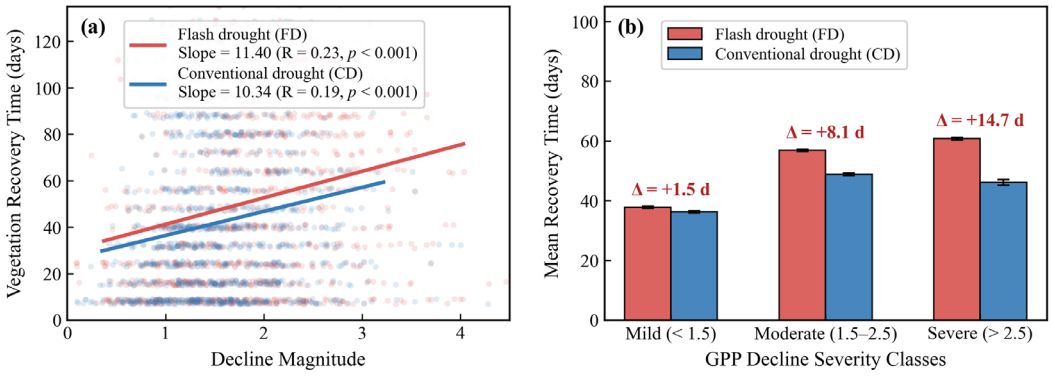

Figure 7. Relationships between vegetation GPP decline magnitude and recovery time under flash droughts and conventional droughts. Panel (**a**) illustrates the linear regression fitting lines between GPP decline magnitude and recovery time in days under flash droughts and conventional droughts. Panel (**b**) compares the mean recovery times between the two drought categories across three GPP decline severity tiers: mild (decline < 1.5), moderate (decline 1.5–2.5), and severe (decline > 2.5).

3.3. Key Driving Factors of Vegetation Recovery Time

To identify the key drivers governing post-drought vegetation recovery time, separate XGBoost models coupled with SHAP analysis were developed for flash and conventional droughts (2000–2022), integrating three drought attributes and six recovery-period hydrothermal anomalies. Evaluated via spatial-temporal cross-validation, the models achieved determination coefficients (R^2) of 0.812 for flash droughts and 0.834 for conventional droughts. Figure 8 presents the relative importance ranking and directional effects of these drivers based on the SHAP analysis.

Under both drought categories, cumulative soil moisture anomaly during the recovery period (SMrec) was the most important explanatory factor, reaching relative contribution rates of 62.09% in the flash drought model and 66.81% in the conventional drought model, well above all other environmental variables. In the flash drought model, the relative contributions of the remaining factors ranked in descending order as follows: recovery air temperature (TEMrec) at 7.39%, drought intensity (DI) at 6.82%, recovery solar radiation (RADrec) at 5.58%, recovery precipitation (PRErec) at 5.23%, recovery

actual evapotranspiration (ETrec) at 4.54%, recovery vapor pressure deficit (VPDrec) at 4.01%, drought duration (DD) at 2.36%, and drought frequency (DF) at 1.99%.

In the conventional drought model, the contributions of the remaining variables ranked in descending order as follows: DI at 8.04%, VPDrec at 7.31%, RADrec at 4.36%, ETrec at 4.14%, TEMrec at 3.79%, PRErec at 3.65%, DD at 1.62%, and DF at 0.28%. Comparing the two models reveals that SMrec played a dominant role under both regimes, with DI ranking second under conventional droughts and third under flash droughts, whereas DD and DF contributed little directly to recovery duration. The primary divergence between the two models appeared in the ranking of atmospheric hydrothermal factors during the recovery period. In the flash drought model, the contributions of TEMrec and RADrec ranked higher than that of VPDrec. Conversely, in the conventional drought model, VPDrec ranked third at 7.31%, showing an importance that was higher than the contributions of TEMrec, RADrec, ETrec, and PRErec.

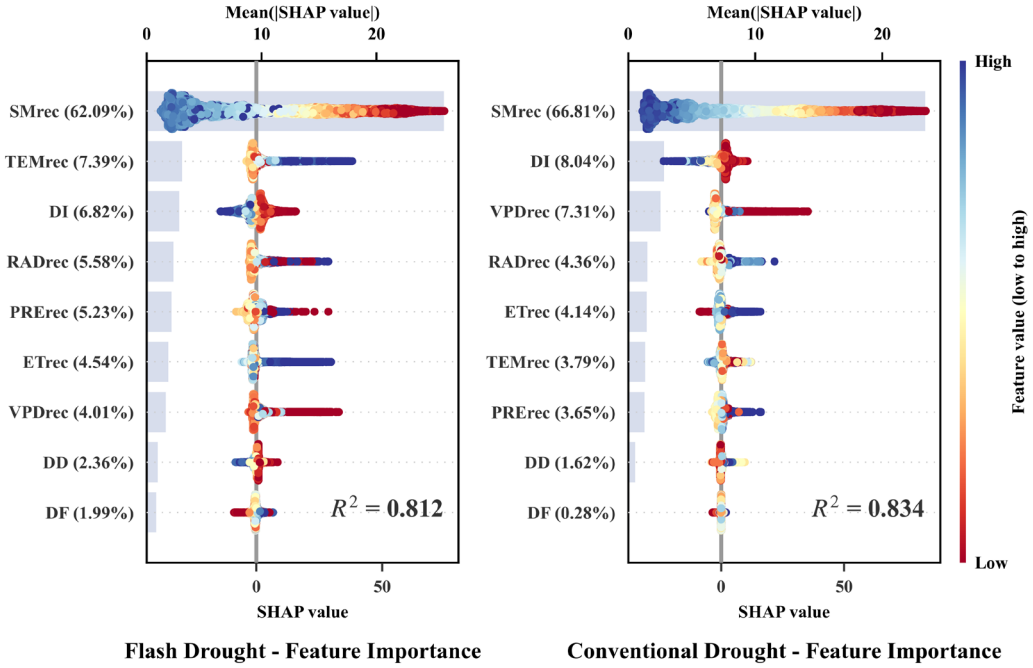

Figure 8. Relative importance and effects of driving factors governing vegetation recovery time under flash and conventional droughts. The light-blue horizontal bars (top axis) represent the mean absolute SHAP values (in days), with relative contribution percentages shown in parentheses. The beeswarm plots (bottom axis) illustrate the directional impact of each driver on recovery duration, where each dot denotes an individual drought event. The right color bar represents feature values ranging from low (red) to high (blue). R^2 values indicate the model generalization performance evaluated via 5 × 5 spatiotemporal cross-validation.

4. Discussion

4.1. Spatiotemporal Evolution and Feature Differences Between Flash and Conventional Droughts

Threshold selection is a key prerequisite for comparing the spatiotemporal characteristics of flash and conventional droughts, as it directly affects event identification. Within the soil moisture decline-rate framework, changes in the onset-rate threshold, minimum event duration, or soil moisture percentile thresholds can alter the screening criteria and the number of identified events. Nevertheless, the overall spatial patterns and associated physical processes remain relatively consistent across different threshold settings [44,45]. To date, no universally accepted quantitative threshold criteria

for flash drought identification have been established in the academic community. Researchers should select appropriate threshold schemes according to their specific scientific questions [46].

This study found that the occurrence frequency of flash droughts exhibited a spatial pattern that was generally higher in the north and lower in the south, consistent with previous investigations of drought characteristics across Central Asia [8,16]. This spatial differentiation is related to differences in surface vegetation cover and antecedent soil moisture conditions [31]. In northern and eastern Kazakhstan, dense grassland vegetation and moderate initial soil moisture provide the moisture base for intense transpirational water loss when atmospheric evaporative demand surges, which accelerates soil moisture depletion and precipitates flash droughts through enhanced land–atmosphere coupling [31,47]. In contrast, soil moisture in southern desert areas remains at a low baseline year-round, making it difficult to satisfy the rapid depletion rate threshold [48]. In comparison, conventional droughts displayed a more uniform spatial distribution [8], reflecting that their formation depends more on large-scale atmospheric circulation anomalies rather than local land–atmosphere interactions [49].

Regarding temporal trends, the occurrence frequency and duration of both drought types showed significant upward trends from 1980 to 2022, with the growth rate of flash drought frequency being approximately 1.56 times that of conventional droughts. This pattern is consistent with global observations indicating an accelerated transition from slow-onset droughts toward flash droughts [11,14]. Pronounced warming across Central Asia in recent years has intensified atmospheric moisture deficits [6], which in turn accelerates drought onset and shortens development times [11,13]. Although drought intensity exhibited multidecadal fluctuations modulated by internal climate variability [6], the deeper deficit depth of flash droughts demonstrates that despite their shorter durations, they induce more severe instantaneous hydrological stress on terrestrial systems [12,13].

4.2. Differences in Productivity Loss and Recovery Trajectories Between Drought Types

The stronger productivity losses and slower recovery under flash droughts across Central Asia corroborate global and Northern Hemisphere findings that rapid-onset droughts amplify carbon losses and delay recovery [14,19,42], as well as regional findings linking recovery duration to damage severity [25,32]. However, recovery in Central Asian drylands is generally more protracted than in humid regions such as southern China and Europe [17,28,32], where abundant moisture accelerates repair, whereas low baseline soil water and high aridity prolong legacy effects [14,31]. Cross-study differences also reflect dataset and methodological choices: satellite GPP captures rapid photosynthetic declines distinct from structural greenness [29], while sub-seasonal soil-moisture screening isolates acute stress masked by monthly meteorological or annual metrics [8,16,29].

These contrasting trajectories stem from distinct physiological stress pathways. Although conventional droughts last longer, their gradual onset allows time for stomatal regulation, osmotic adjustment, and carbon reallocation, mitigating acute injury [50,51]. Conversely, flash droughts induce abrupt soil desiccation under high evaporative demand, outpacing stomatal defense and triggering hydraulic failure and leaf wilting [20,21,31], which deepens damage and prolongs subsequent tissue repair [19,22,23].

Biome divergences further reflect contrasting rooting and water-use strategies. Forests experienced the sharpest declines during flash droughts because strong canopy–atmosphere coupling pushes transpirational demand beyond hydraulic safety limits [23,52,53], though deep roots and woody carbon reserves aid faster rebound. By contrast, shallow-rooted croplands and grasslands recovered slowest after flash droughts in Central Asia. Although herbaceous biomes often rebound faster than forests in global or wetter regions owing to simpler structures [23,32], rapid upper-soil desiccation in

drylands severely impairs crops and grasses that rely primarily on topsoil moisture recharge, suppressing recovery [28]. Notably, shrublands showed weaker sensitivity to flash droughts and similar recovery times across both regimes: deep taproots and conservative stomatal control buffer brief flash-drought shocks [27], whereas prolonged conventional droughts gradually exhaust deep soil water reserves.

4.3. Influencing Factors of Vegetation Recovery Time Across Different Drought Regimes

The overriding control of post-drought soil moisture replenishment on vegetation recovery aligns with global and regional findings that soil water availability governs ecosystem resilience [22,23,25,32]. Consistent with evidence that soil moisture sensitivity peaks in water-limited biomes [23], its dominance in arid Central Asia is stronger than in humid or energy-limited regions where temperature and radiation co-regulate recovery [18,32]. Ecohydrologically, soil moisture represents the direct plant-available water pool, whereas dryland precipitation is heavily lost to evaporation, interception, and runoff before recharging the soil profile. Atmospheric conditions or rainfall pulses alone therefore cannot restore photosynthesis unless soil water deficits ease. Replenishing soil moisture restores xylem water potential, cell turgor, and stomatal conductance, enabling enzymatic reactivation and foliar regrowth [23,25,32]. Meanwhile, drought intensity reflects legacy hydraulic and structural damage [22,28], whereas drought duration and frequency act mainly indirectly through cumulative moisture depletion.

Secondary atmospheric bottlenecks further diverge across drought regimes. Once brief flash droughts subside and water stress eases, photosynthetic recovery is largely regulated by temperature and solar radiation, which drive enzymatic activity and tissue repair [18,32]. By contrast, after prolonged conventional droughts marked by chronic desiccation, elevated atmospheric vapor pressure deficit forces plants to maintain conservative stomatal closure to prevent further hydraulic failure, constraining carbon assimilation and slowing recovery [5,54]. Ultimately, interpretable nonlinear attribution disentangles collinear hydroclimatic controls and reveals how regime-specific moisture–energy–atmosphere constraints shape dryland recovery [28,33].

4.4. Limitations and Future Work

Although this study provides systematic insights into vegetation vulnerability and recovery across Central Asia, several limitations should be acknowledged. First, aggregating 30 m land-cover data to a 0.1° grid inevitably introduces mixed-pixel effects, which may smooth out localized vegetation responses across narrow ecotones. Second, our calendar-based GPP standardization removes only climatological seasonality; it cannot fully separate interannual phenological shifts from drought-induced GPP drops, which may introduce residual uncertainty [55]. Third, satellite GPP captures canopy-level productivity but misses belowground biomass allocation and deep groundwater buffering in deep-rooted vegetation. Fourth, potential sample selection bias may arise from event screening and recovery tracking: the initial screening excluded similar proportions of flash drought (FD) and conventional drought (CD) events, at 69.46% and 68.62%, respectively, whereas during recovery tracking, 24.99% of FD events and 29.17% of CD events were excluded as unrecovered.

Future work should integrate high-resolution microwave soil moisture and solar-induced chlorophyll fluorescence (SIF) with in situ flux tower and tree-ring observations. Additionally, coupling dynamic phenological baselines with ecohydrological models will be essential for evaluating ecosystem resilience under future climate scenarios (e.g., SSPs).

5. Conclusions

Using ERA5-Land soil moisture from 1980 to 2022 and GLASS GPP from 2000 to 2022, this study compared flash and conventional droughts across Central Asia. Over the past four decades, both drought types increased significantly in frequency and duration. Flash droughts occurred nearly twice as often, with high-frequency zones concentrated in northern and eastern Central Asia. Although shorter-lived, flash droughts were 3.5 times more intense on average than conventional droughts. Consequently, flash droughts caused larger overall GPP decline magnitudes, averaging 1.875 versus 1.602 standardized anomaly units. They also prolonged post-drought recovery to 50.79 days, compared with 42.19 days after conventional droughts. Biome responses varied across the region. Forests, croplands, and grasslands suffered greater GPP losses during flash droughts, whereas shrublands declined more under conventional droughts. Post-drought recovery was significantly prolonged after flash droughts across croplands, grasslands, and forests, whereas shrublands exhibited similar recovery durations under both regimes. Recovery duration also lengthened as productivity damage deepened, and the recovery gap between drought types widened under severe stress. Spatiotemporal cross-validation confirmed strong model performance in simulating recovery time, with R^2 values of 0.812 for flash droughts and 0.834 for conventional droughts. SHAP analysis showed that cumulative recovery-period soil moisture anomaly dominated recovery under both regimes, contributing 62.09% for flash droughts and 66.81% for conventional droughts. Drought intensity ranked second under conventional droughts and third under flash droughts, while drought duration and frequency played minor roles. Secondary recovery-period atmospheric drivers differed between regimes. Air temperature and solar radiation were more influential for flash droughts, whereas vapor pressure deficit ranked third for conventional droughts.

Several uncertainties remain. Aggregating 30 m land-cover maps to a 0.1° grid introduces mixed-pixel bias. Fixed calendar baselines for GPP standardization cannot fully isolate drought impacts from interannual phenological shifts. In addition, canopy-level GPP overlooks belowground carbon allocation and deep groundwater buffering. Future studies should combine high-resolution microwave soil moisture, solar-induced chlorophyll fluorescence, and in situ flux or tree-ring records within dynamic phenological frameworks to better project dryland resilience.

Author Contributions: Conceptualization, Y.C. and J.G.; methodology, J.G. and Y.L.; software, J.G.; validation, J.G., Y.L., Y.Y., G.F., Z.L., J.Q. and F.S.; formal analysis, J.G., Y.L., Y.Y., G.F., Z.L., J.Q. and F.S.; investigation, J.G., Y.L., Y.Y., G.F., Z.L., J.Q. and F.S.; resources, Y.C.; data curation, J.G., Y.L., Y.Y., G.F., Z.L., J.Q. and F.S.; writing—original draft preparation, J.G.; writing—review and editing, Y.C., J.G., Y.L., Y.Y., G.F., Z.L., J.Q. and F.S.; visualization, J.G.; supervision, Y.C.; project administration, Y.C.; funding acquisition, Y.C., Y.L. and F.S. All authors have read and agreed to the published version of the manuscript.

Funding: This research was funded by the National Natural Science Foundation of China (grant number W2412135), the Natural Science Foundation of Xinjiang Uygur Autonomous Region (grant number 2025D01B165), and the Tianchi Talent Program of Xinjiang, China.

Data Availability Statement: The datasets used in this study are openly accessible to the public. The ERA5-Land reanalysis data were retrieved from the ECMWF Copernicus Climate Data Store at https://cds.climate.copernicus.eu/datasets/reanalysis-era5-land (accessed on 19 February 2026). The Global Land Surface Satellite (GLASS) products were obtained from the GLASS product repository at Beijing Normal University at https://glass-product.bnu.edu.cn/ (accessed on 4 January 2026). The 30 m Global Land Cover product with Fine Classification System (GLC_FCS30D) was downloaded from the Zenodo repository at https://zenodo.org/records/8239305 (accessed on 30 May 2026).

https://doi.org/10.3390/rs18234065

Acknowledgments: We are sincerely grateful to the reviewers and editors for their constructive comments for the improvement of the manuscript.

Conflicts of Interest: The authors declare no conflicts of interest.

References

1. Zscheischler, J.; Westra, S.; van den Hurk, B.J.J.M.; Seneviratne, S.I.; Ward, P.J.; Pitman, A.; AghaKouchak, A.; Bresch, D.N.; Leonard, M.; Wahl, T.; et al. Future climate risk from compound events. *Nat. Clim. Change* **2018**, *8*, 469–477.
2. Xu, C.; McDowell, N.G.; Fisher, R.A.; Wei, L.; Sevanto, S.; Christoffersen, B.O.; Weng, E.; Middleton, R.S. Increasing impacts of extreme droughts on vegetation productivity under climate change. *Nat. Clim. Change* **2019**, *9*, 948–953.
3. Li, W.; Pacheco-Labrador, J.; Migliavacca, M.; Miralles, D.; Hoek van Dijke, A.; Reichstein, M.; Forkel, M.; Zhang, W.; Frankenberg, C.; Panwar, A.; et al. Widespread and complex drought effects on vegetation physiology inferred from space. *Nat. Commun.* **2023**, *14*, 4640.
4. Huang, J.; Yu, H.; Guan, X.; Wang, G.; Guo, R. Accelerated dryland expansion under climate change. *Nat. Clim. Change* **2015**, *6*, 166–171.
5. Yao, Y.; Fu, B.; Liu, Y.; Zhang, Y.; Ding, J.; Li, Y.; Zhou, S.; Song, J.; Wang, S.; Li, C.; et al. Compound hot–dry events greatly prolong the recovery time of dryland ecosystems. *Natl. Sci. Rev.* **2024**, *11*, nwae274.
6. Jiang, J.; Zhou, T. Agricultural drought over water-scarce Central Asia aggravated by internal climate variability. *Nat. Geosci.* **2023**, *16*, 154–161.
7. Chen, F.; Wang, J.; Jin, L.; Zhang, Q.; Li, J.; Chen, J. Rapid warming in mid-latitude central Asia for the past 100 years. *Front. Earth Sci. China* **2009**, *3*, 42–50.
8. Zhu, Y.; Yang, P.; Huang, H.; Xia, J.; Chen, Y.; Li, Z.; Shi, X. How is about the flash drought events and their impacts on vegetation in Central Asia. *Clim. Dyn.* **2024**, *62*, 7073–7093.
9. Jiang, L.; Bao, A.; Jiapaer, G.; Liu, R.; Yuan, Y.; Yu, T. Monitoring land degradation and assessing its drivers to support sustainable development goal 15.3 in Central Asia. *Sci. Total Environ.* **2022**, *807*, 150868.
10. Pendergrass, A.G.; Meehl, G.A.; Pulwarty, R.; Hobbins, M.; Hoell, A.; AghaKouchak, A.; Bonfils, C.J.W.; Gallant, A.J.E.; Hoerling, M.; Hoffmann, D.; et al. Flash droughts present a new challenge for subseasonal-to-seasonal prediction. *Nat. Clim. Change* **2020**, *10*, 191–199.
11. Yuan, X.; Wang, Y.M.; Ji, P.; Wu, P.L.; Sheffield, J.; Otkin, J.A. A global transition to flash droughts under climate change. *Science* **2023**, *380*, 187–191.
12. Otkin, J.A.; Svoboda, M.; Hunt, E.D.; Ford, T.W.; Anderson, M.C.; Hain, C.; Basara, J.B. Flash Droughts: A Review and Assessment of the Challenges Imposed by Rapid-Onset Droughts in the United States. *Bull. Am. Meteorol. Soc.* **2018**, *99*, 911–919.
13. Qing, Y.; Wang, S.; Ancell, B.C.; Yang, Z.-L. Accelerating flash droughts induced by the joint influence of soil moisture depletion and atmospheric aridity. *Nat. Commun.* **2022**, *13*, 1139.
14. Guo, R.; Wu, X.; Wang, P.; Chen, T.; Chen, X.; Cai, J.; Wang, X.; Zhang, Z.; Meng, Z.; Liu, Y. Increased spread of global flash droughts threatens vegetation productivity resilience. *Nat. Commun.* **2026**, *17*, 4050.
15. Guo, H.; Bao, A.; Liu, T.; Jiapaer, G.; Ndayisaba, F.; Jiang, L.; Kurban, A.; De Maeyer, P. Spatial and temporal characteristics of droughts in Central Asia during 1966–2015. *Sci. Total Environ.* **2018**, *624*, 1523–1538.
16. Zhu, Y.; Yang, P.; Xia, J.; Huang, H.; Chen, Y.; Li, L.; Sun, K.; Song, J.; Shi, X.; Lu, X. Differential impact of flash droughts on water use efficiency in terrestrial ecosystems in Central Asia. *Clim. Change* **2025**, *178*, 53.
17. O, S.; Park, S.K. Flash drought drives rapid vegetation stress in arid regions in Europe. *Environ. Res. Lett.* **2023**, *18*, 014028.
18. Zhang, S.; Yang, Y.; Wu, X.; Li, X.; Shi, F. Postdrought Recovery Time Across Global Terrestrial Ecosystems. *J. Geophys. Res. Biogeosciences* **2021**, *126*, e2020JG005699.
19. Chai, Y.; Miao, C.; AghaKouchak, A.; Pokhrel, Y.; Fu, Y.; Li, X.; Ji, J.; Zhang, Q.; Peñuelas, J. Flash droughts exacerbate global vegetation loss and delay recovery. *Nat. Commun.* **2025**, *17*, 485.
20. Martin-StPaul, N.; Delzon, S.; Cochard, H.; Maherali, H. Plant resistance to drought depends on timely stomatal closure. *Ecol. Lett.* **2017**, *20*, 1437–1447.
21. Zhang, M.; Yuan, X. Rapid reduction in ecosystem productivity caused by flash droughts based on decade-long FLUXNET observations. *Hydrol. Earth Syst. Sci.* **2020**, *24*, 5579–5593.
22. Schwalm, C.R.; Anderegg, W.R.L.; Michalak, A.M.; Fisher, J.B.; Biondi, F.; Koch, G.; Litvak, M.; Ogle, K.; Shaw, J.D.; Wolf, A.; et al. Global patterns of drought recovery. *Nature* **2017**, *548*, 202–205.

23. Yao, Y.; Liu, Y.; Zhou, S.; Song, J.; Fu, B. Soil moisture determines the recovery time of ecosystems from drought. *Glob. Change Biol.* **2023**, *29*, 3562–3574.
24. Anderegg, W.R.; Schwalm, C.; Biondi, F.; Camarero, J.J.; Koch, G.; Litvak, M.; Ogle, K.; Shaw, J.D.; Shevliakova, E.; Williams, A. Pervasive drought legacies in forest ecosystems and their implications for carbon cycle models. *Science* **2015**, *349*, 528–532.
25. Wang, C.; Chen, J.; Lee, S.-C.; Xiong, L.; Su, T.; Lin, Q.; Xu, C.-Y. Response and recovery times of vegetation productivity under drought stress: Dominant factors and relationships. *J. Hydrol.* **2025**, *655*, 132945.
26. Lenton, T.M.; Held, H.; Kriegler, E.; Hall, J.W.; Lucht, W.; Rahmstorf, S.; Schellnhuber, H.J. Tipping elements in the Earth's climate system. *Proc. Natl. Acad. Sci. USA* **2008**, *105*, 1786–1793.
27. Brunner, I.; Herzog, C.; Dawes, M.A.; Arend, M.; Sperisen, C. How tree roots respond to drought. *Front. Plant Sci.* **2015**, *6*, 547.
28. Lu, M.; Sun, H.; Cheng, L.; Li, S.; Qin, H.; Yi, S.; Zhang, H.; Zhang, W. Heterogeneity in vegetation recovery rates post-flash droughts across different ecosystems. *Environ. Res. Lett.* **2024**, *19*, 074028.
29. Wu, G.; Jiang, L.; Li, Q.; Tan, Z.; Liu, W.; Gui, X. Higher post-drought recovery capacity of vegetation productivity compared to greenness in Central Asia. *J. Environ. Manag.* **2025**, *390*, 126214.
30. Lloret, F.; Keeling, E.G.; Sala, A. Components of tree resilience: Effects of successive low-growth episodes in old ponderosa pine forests. *Oikos* **2011**, *120*, 1909–1920.
31. O, S.; Park, S.K. Global ecosystem responses to flash droughts are modulated by background climate and vegetation conditions. *Commun. Earth Environ.* **2024**, *5*, 88.
32. Lu, M.; Sun, H.; Yang, Y.; Xue, J.; Ling, H.; Zhang, H.; Zhang, W. Assessing recovery time of ecosystems in China: Insights into flash drought impacts on gross primary productivity. *Hydrol. Earth Syst. Sci.* **2025**, *29*, 613–625.
33. Lundberg, S.M.; Lee, S.-I. A unified approach to interpreting model predictions. In Proceedings of the 31st International Conference on Neural Information Processing Systems, Long Beach, CA, USA, 4–9 December 2017; pp. 4768–4777.
34. Xu, P.; Wang, L.; Ming, J. Central Asian Precipitation Extremes Affected by an Intraseasonal Planetary Wave Pattern. *J. Clim.* **2022**, *35*, 2603–2616.
35. Zhou, Y.; Zhang, L.; Fensholt, R.; Wang, K.; Vitkovskaya, I.; Tian, F. Climate Contributions to Vegetation Variations in Central Asian Drylands: Pre- and Post-USSR Collapse. *Remote Sens.* **2015**, *7*, 2449–2470.
36. Li, M.; Yao, J.; Zheng, J. Spatio-Temporal Change and Drivers of the Vegetation Trends in Central Asia. *Forests* **2024**, *15*, 1416.
37. Muñoz-Sabater, J.; Dutra, E.; Agustí-Panareda, A.; Albergel, C.; Arduini, G.; Balsamo, G.; Boussetta, S.; Choulga, M.; Harrigan, S.; Hersbach, H.; et al. ERA5-Land: A state-of-the-art global reanalysis dataset for land applications. *Earth Syst. Sci. Data* **2021**, *13*, 4349–4383.
38. Liang, S.L.; Cheng, J.; Jia, K.; Jiang, B.; Liu, Q.; Xiao, Z.Q.; Yao, Y.J.; Yuan, W.P.; Zhang, X.T.; Zhao, X.; et al. The Global Land Surface Satellite (GLASS) Product Suite. *Bull. Am. Meteorol. Soc.* **2021**, *102*, E323–E337.
39. Allen, R.G.; Pereira, L.S.; Raes, D.; Smith, M. *Crop Evapotranspiration: Guidelines for Computing Crop Water Requirements*; FAO Irrigation and Drainage Paper No. 56; Food and Agriculture Organization of the United Nations: Rome, Italy, 1998; p. e156.
40. Zhang, X.; Liu, L.; Chen, X.; Gao, Y.; Xie, S.; Mi, J. GLC_FCS30: Global land-cover product with fine classification system at 30 m using time-series Landsat imagery. *Earth Syst. Sci. Data* **2021**, *13*, 2753–2776.
41. Yuan, X.; Wang, L.; Wu, P.; Ji, P.; Sheffield, J.; Zhang, M. Anthropogenic shift towards higher risk of flash drought over China. *Nat. Commun.* **2019**, *10*, 4661.
42. Zhang, M.; Yuan, X.; Zeng, Z.; Pan, M.; Wu, P.; Xiao, J.; Keenan, T.F. A pronounced decline in northern vegetation resistance to flash droughts from 2001 to 2022. *Nat. Commun.* **2025**, *16*, 2984.
43. Osman, M.; Zaitchik, B.F.; Badr, H.S.; Christian, J.I.; Tadesse, T.; Otkin, J.A.; Anderson, M.C. Flash drought onset over the contiguous United States: Sensitivity of inventories and trends to quantitative definitions. *Hydrol. Earth Syst. Sci.* **2021**, *25*, 565–581.
44. Ford, T.W.; Labosier, C.F. Meteorological conditions associated with the onset of flash drought in the Eastern United States. *Agric. For. Meteorol.* **2017**, *247*, 414–423.
45. Xiao, X.; Flanagan, P.X.; Wakefield, R.A.; Hunt, E.D.; Otkin, J.A.; Basara, J.B.; Christian, J.I. A Methodology for Flash Drought Identification: Application of Flash Drought Frequency across the United States. *J. Hydrometeorol.* **2019**, *20*, 833–846.
46. Lisonbee, J.; Woloszyn, M.; Skumanich, M. Making sense of flash drought: Definitions, indicators, and where we go from here. *J. Appl. Serv. Climatol.* **2021**, *2021*, 1–19.
47. Chen, L.; Ford, T.W.; Yadav, P. The Role of Vegetation in Flash Drought Occurrence: A Sensitivity Study Using Community Earth System Model, Version 2. *J. Hydrometeorol.* **2021**, *22*, 845–857.
48. Mukherjee, S.; Mishra, A.K. A Multivariate Flash Drought Indicator for Identifying Global Hotspots and Associated Climate Controls. *Geophys. Res. Lett.* **2022**, *49*, e2021GL096804.

49. Barlow, M.; Zaitchik, B.; Paz, S.; Black, E.; Evans, J.; Hoell, A. A Review of Drought in the Middle East and Southwest Asia. *J. Clim.* **2016**, *29*, 8547–8574.
50. He, B.; Liu, J.; Guo, L.; Wu, X.; Xie, X.; Zhang, Y.; Chen, C.; Zhong, Z.; Chen, Z. Recovery of Ecosystem Carbon and Energy Fluxes From the 2003 Drought in Europe and the 2012 Drought in the United States. *Geophys. Res. Lett.* **2018**, *45*, 4879–4888.
51. Wei, M.; Jiao, L.; Zhang, P.; Xue, R.; Wang, X.; Li, Q.; Jin, M. Spatial and temporal characteristics of vegetation resilience to drought in China. *Sci. China Earth Sci.* **2025**, *68*, 2310–2327.
52. McDowell, N.; Pockman, W.T.; Allen, C.D.; Breshears, D.D.; Cobb, N.; Kolb, T.; Plaut, J.; Sperry, J.; West, A.; Williams, D.G.; et al. Mechanisms of plant survival and mortality during drought: Why do some plants survive while others succumb to drought? *New Phytol.* **2008**, *178*, 719–739.
53. Wu, T.; Liu, Y.; Chen, L.; Fu, Z.; Fu, B.; Li, Y.; Wu, X.; Ding, J.; Li, C.; Wang, S.; et al. Human pressure and biodiversity modify forest resilience after extreme multi-year droughts. *Nat. Ecol. Evol.* **2026**, *10*, 880–892.
54. Grossiord, C.; Buckley, T.N.; Cernusak, L.A.; Novick, K.A.; Poulter, B.; Siegwolf, R.T.W.; Sperry, J.S.; McDowell, N.G. Plant responses to rising vapor pressure deficit. *New Phytol.* **2020**, *226*, 1550–1566.
55. Mulualem, G.M.; Dash, J. The impact of phenological shifts on carbon uptake across major terrestrial biomes. *Carbon Balance Manag.* **2026**, *21*, 95.

Disclaimer/Publisher's Note: The statements, opinions and data contained in all publications are solely those of the individual author(s) and contributor(s) and not of MDPI and/or the editor(s). MDPI and/or the editor(s) disclaim responsibility for any injury to people or property resulting from any ideas, methods, instructions or products referred to in the content.

https://doi.org/10.3390/rs18234065